



# Using Multiple Emission Line Ratios to Constrain the Slope of the Dust Attenuation Law

Moire K. M. Prescott<sup>1</sup> , Kristian M. Finlator<sup>1</sup> , Nikko J. Cleri<sup>2,3</sup> , Jonathan R. Trump<sup>4</sup> , and Casey Papovich<sup>2,3</sup> <sup>1</sup> Department of Astronomy, New Mexico State University, P.O. Box 30001, MSC 4500, Las Cruces, NM 88003, USA; [mkpresco@nmsu.edu](mailto:mkpresco@nmsu.edu)<sup>2</sup> Department of Physics and Astronomy, Texas A&M University, College Station, TX 77843-4242, USA<sup>3</sup> George P. and Cynthia Woods Mitchell Institute for Fundamental Physics and Astronomy, Texas A&M University, College Station, TX 77843-4242, USA<sup>4</sup> Department of Physics, University of Connecticut, 196A Auditorium Road, Unit 3046, Storrs, CT 06269, USA

Received 2021 July 12; revised 2022 January 18; accepted 2022 February 7; published 2022 March 28

## Abstract

We explore the possibility and practical limitations of using a three-line approach to measure both the slope and normalization of the dust attenuation law in individual galaxies. To do this, we focus on a sample of 11 galaxies with existing ground-based Balmer  $H\alpha$  and  $H\beta$  measurements from slit spectra, plus space-based grism constraints on Paschen- $\beta$ . When accounting for observational uncertainties, we show that one galaxy has a well-constrained dust-law slope and normalization in the range expected from theoretical arguments; this galaxy therefore provides an example of what may be possible in the future. However, most of the galaxies are best fit by unusually steep or shallow slopes. We then explore whether additional astrophysical effects or observational biases could explain the elevated Paschen- $\beta/H\alpha$  ratios driving these results. We find that galaxies with high Paschen- $\beta/H\alpha$  ratios may be explained by slightly sub-unity covering fractions ( $>97\%$ ). Alternatively, differing slit losses for different lines can have a large impact on the results, emphasizing the importance of measuring all three lines with a consistent spectroscopic aperture. We conclude that, while the three-line approach to constraining the shape of the dust attenuation law in individual galaxies is promising, deep observations and a consistent observational strategy will be required to minimize observational biases and to disentangle the astrophysically interesting effect of differing covering fractions. The James Webb Space Telescope will provide more sensitive measurements of Balmer and Paschen lines for galaxies at  $z \approx 0.3$ – $2$ , enabling uniform constraints on the optical–infrared dust attenuation law and its intrinsic variation.

*Unified Astronomy Thesaurus concepts:* [Interstellar dust extinction \(837\)](#); [Interstellar dust \(836\)](#); [Astrophysical dust processes \(99\)](#); [Emission line galaxies \(459\)](#); [Galaxies \(573\)](#)

## 1. Introduction

Dust attenuation is an important factor in interpreting observations of galaxies. This is particularly true for high-redshift galaxies, for which our primary observational constraints are confined to the rest-frame ultraviolet where the effect of dust extinction is particularly strong. Our ability to account for dust affects the accuracy of derived galaxy properties such as the implied star formation rates, ionization parameters, and gas-phase metallicities. Complicating the situation further, studies have uncovered evidence that the dust law in galaxies is not universal, neither among members of the Local Group (e.g., Pei 1992; Gordon et al. 2003) nor at higher redshifts ( $z \sim 0.5$ – $3.0$ ; Kriek & Conroy 2013; Salmon et al. 2016).

Correcting an observed quantity for the effects of dust requires understanding both the amount of dust along the line of sight and the amount of extinction that dust causes as a function of wavelength, i.e., the dust extinction law, which is related to the dust composition and distribution of grain sizes. When considering an entire galaxy, it is often more accurate to use the term “attenuation” to describe the effects of dust (e.g., Calzetti 2001; Salim & Narayanan 2020). Whereas dust extinction is the removal of light from the line of sight due to absorption and scattering by dust, dust attenuation encompasses the contributions of absorption plus scattering both out of and back into the line of sight.

In practice, it is nontrivial to determine the dust attenuation for distant galaxies. Typically, the ratio of two nebular lines with a known intrinsic ratio is used to estimate the amount of dust attenuation, which is then used to scale a dust attenuation law (the curve representing dust attenuation versus wavelength) of an assumed shape. The popular Balmer decrement method, for example, involves the observed flux ratio of the  $H\alpha$   $\lambda 6563$  Å and  $H\beta$   $\lambda 4861$  Å lines, while ratios of longer-wavelength hydrogen lines in the Paschen and Brackett series have also been explored for sightlines to nearby star-forming regions (Puxley & Brand 1994; Petersen & Gammelgaard 1997; Greve 2010). Commonly used empirical attenuation curves include the prescriptions of Cardelli et al. (1989), based on measurements of individual stars in the Milky Way, and Calzetti et al. (1999), derived using a sample of local starburst galaxies. Charlot & Fall (2000) showed that a power-law dust attenuation law in which the optical depth  $\tau_\lambda$  is proportional to  $\lambda^{-n}$  is successful at reproducing observations of starburst galaxies, with the exponent  $n$  being sensitive to whether the radiation is emitted from the diffuse interstellar medium ( $n \sim 0.7$ ) versus from stars embedded in their birth clouds ( $n \sim 1.3$ ). This flexible attenuation law has been implemented in spectral energy distribution fitting codes (e.g., the Code Investigating GALaxy Emission, CIGALE; Boquien et al. 2019).

Under physically plausible assumptions about nebular conditions (electron density,  $n_e$ , and temperature,  $T_e$ ), combining constraints on  $H\alpha$  and  $H\beta$  with an additional nebular hydrogen line at a wide wavelength separation from the other two, e.g., a Paschen series line in the near-infrared, can provide separate measurements of the dust attenuation at two different



Original content from this work may be used under the terms of the [Creative Commons Attribution 4.0 licence](#). Any further distribution of this work must maintain attribution to the author(s) and the title of the work, journal citation and DOI.

wavelengths, and in principle, therefore, constrain both the normalization and the slope of the dust attenuation law within an individual galaxy. While conceptually straightforward, the approach has not seen widespread use. This is likely due to the fact that Paschen series lines are in the rest-frame near-infrared and are intrinsically weaker than the strong Balmer lines in the rest-frame optical. As a result, Paschen emission line flux measurements have been published for only a handful of galaxies. For example, HST/NICMOS was used to obtain Paschen- $\alpha$  ( $\text{Pa}\alpha$ ;  $\lambda = 1.875 \mu\text{m}$ ) imaging of local galaxies (Alonso-Herrero et al. 2006; Calzetti et al. 2007; Kennicutt et al. 2007), although these data covered only the central  $1'$  of each galaxy. The full disks of two nearby galaxies were imaged more recently in Paschen- $\beta$  ( $\text{Pa}\beta$ ;  $\lambda = 1.2822 \mu\text{m}$ ) using HST/WFC3 (Kessler et al. 1919). Further afield, a recent study combined measurements of ground-based  $\text{H}\alpha$  and  $\text{H}\beta$  line measurements with  $\text{Pa}\beta$  constraints obtained with the HST/WFC3 grism for 11 galaxies at  $z \approx 0.2$  (Cleri et al. 2020). Some of these galaxies showed extreme ratios of  $\text{Pa}\beta$  to  $\text{H}\alpha$ , raising a range of possibilities such as varying covering fractions, underestimated slit loss corrections, or unusual dust laws. At higher redshifts ( $z > 2$ ),  $\text{Pa}\alpha$  measurements have been reported for a handful of individual lensed galaxies (Papovich et al. 2009; Finkelstein et al. 2011; Shipley et al. 2016).

In this paper, we explore what constraints on three nebular lines (specifically  $\text{H}\alpha$ ,  $\text{H}\beta$ , and  $\text{Pa}\beta$ ) can tell us about the range of dust laws in the sample of 11  $z \approx 0.2$  galaxies (Cleri et al. 2020). In Section 2, we introduce the observed galaxy sample, as well as the emission line fluxes and galaxy morphology measurements that will be used in our analysis. We explore the implied constraints on dust-law slopes and normalizations for the galaxy sample using an analytic approach in Section 3. In Section 4, we estimate the implied dust-law parameters after folding in observational uncertainties, and then in Section 5, we explore whether additional astrophysical or observational effects could be biasing the observed line ratios. We discuss the implications of these results for the utility and reliability of the three-line method in Section 6, and we conclude in Section 7. For consistency with Cleri et al. (2020), we assume a WMAP9 cosmology ( $\Omega_M = 0.287$ ,  $\Omega_\Lambda = 0.713$ ,  $h = 0.693$ ); the angular scale at  $z \approx 0.2$  is  $3.3 \text{ kpc}/''$ . We also assume the intrinsic emission line ratios appropriate for Case B recombination, i.e.,  $\text{H}\alpha/\text{H}\beta = 2.86$  and  $\text{H}\alpha/\text{Pa}\beta = 17.6$  ( $T = 10^4 \text{ K}$ ,  $n_e = 10^4 \text{ cm}^{-3}$ ), values that are relatively insensitive to density and gas temperature (Osterbrock 1989). Unless otherwise specified, throughout this paper we use  $\tau_V$  to refer to the nebular attenuation, which is typically a factor of  $\sim 2$  higher than the attenuation of the stellar continuum (e.g., Calzetti 1997).

## 2. The Target Sample

Cleri et al. (2020) presented a sample of 11 galaxies with flux measurements for all three lines— $\text{Pa}\beta$ ,  $\text{H}\alpha$ , and  $\text{H}\beta$ . The disk-integrated  $\text{Pa}\beta$  flux measurements were derived as part of the CANDELS Ly $\alpha$  Emission at Reionization (CLEAR) survey (HST GO Cycle 23, PI: Papovich; Estrada-Carpenter et al. 2019; Simons et al. 2021; R. C. Simons et al. 2022, in preparation), a HST/WFC3 G102 slitless grism survey of 12 pointings in the GOODS-N and GOODS-S extragalactic fields (Giavalisco et al. 2004), with existing multiband HST imaging from the Cosmic Assembly Near-Infrared Deep Extragalactic Legacy Survey (CANDELS; Grogin et al. 2011;

Koekemoer et al. 2011) and HST/WFC3 G141 grism coverage thanks to the 3D-HST Survey (Brammer et al. 2012; Momcheva et al. 2016). The Balmer line measurements were obtained via ground-based spectroscopy from Keck/DEIMOS using a  $1''$ -wide slit as part of the Team Keck Redshift Survey of the GOODS-N field (Wirth et al. 2004). DEIMOS does not correct for atmospheric dispersion; we note, however, that the typical spatial offset between the  $\text{H}\beta$  and  $\text{H}\alpha$  wavelengths is estimated to be  $\sim 0.5''$  (less than the slitwidth) for  $\sec(z) < 2$ .<sup>5</sup> Since these ground-based data were not flux-calibrated, line fluxes were derived by estimating the equivalent widths of the lines, interpolating broadband photometric magnitudes of the entire galaxy to compute the absolute magnitude in the continuum, and computing the corresponding total galaxy line fluxes (Weiner et al. 2007). This approach was used to account on average for both throughput and slit losses, under the assumption that the equivalent width is constant across the galaxy. No corrections were made for Balmer stellar absorption, since at the spectral resolution of DEIMOS, the narrower Balmer emission lines can be distinguished from the broader underlying absorption profile.

For our analysis, we collected galaxy redshifts and  $\text{Pa}\beta$ ,  $\text{H}\alpha$ , and  $\text{H}\beta$  line fluxes from Cleri et al. (2020), morphological measurements (effective radius  $r_{\text{eff}}$ , Sérsic  $n$ , axis ratio, position angle) for each galaxy from van der Wel et al. (2012), and galaxy stellar mass measurements from Skelton et al. (2014).

## 3. Analytic Approach

With two line ratio measurements ( $\text{H}\alpha/\text{H}\beta$  and  $\text{Pa}\beta/\text{H}\alpha$ ) and two parameters (slope and normalization), it is possible to constrain a galaxy's nebular attenuation law analytically. We start by assuming a uniform dust screen with no slit losses as our baseline scenario. Similar to what is done elsewhere (Charlot & Fall 2000), we parameterize the dust attenuation law using the optical depth as a function of wavelength  $\tau_\lambda$ , scaled to the V-band (5500 Å) optical depth  $\tau_V$ :

$$\tau_\lambda = \tau_V (\lambda/5500 \text{ Å})^{-n}, \quad (1)$$

where  $n$  is the dust-law slope, and the normalization,  $\tau_V$ , can be expressed as  $A_V = 1.086\tau_V$  in magnitudes.

The observed fluxes of the emission lines can then be written as

$$F_i = L_i e^{-\tau_V (\lambda_i/5500 \text{ Å})^{-n}} \times \frac{1}{4\pi d_L^2}, \quad (2)$$

where  $i = [\text{Pa}\beta, \text{H}\alpha, \text{H}\beta]$ , and  $d_L$  is the luminosity distance at the redshift of the galaxy.

The relevant line ratios are therefore

$$\frac{F_{\text{Pa}\beta}/F_{\text{H}\alpha}}{L_{\text{Pa}\beta}/L_{\text{H}\alpha}} = e^{-\tau_V [(\lambda_{\text{Pa}\beta}/5500 \text{ Å})^{-n} - (\lambda_{\text{H}\alpha}/5500 \text{ Å})^{-n}]} \quad (3)$$

$$\frac{F_{\text{H}\alpha}/F_{\text{H}\beta}}{L_{\text{H}\alpha}/L_{\text{H}\beta}} = e^{-\tau_V [(\lambda_{\text{H}\alpha}/5500 \text{ Å})^{-n} - (\lambda_{\text{H}\beta}/5500 \text{ Å})^{-n}]}. \quad (4)$$

Combining these two equations and eliminating  $\tau_V$ , we derive a relationship between the observable line ratios, the

<sup>5</sup> [https://www2.keck.hawaii.edu/inst/newsletters/Vol4/Volume\\_4.html](https://www2.keck.hawaii.edu/inst/newsletters/Vol4/Volume_4.html)

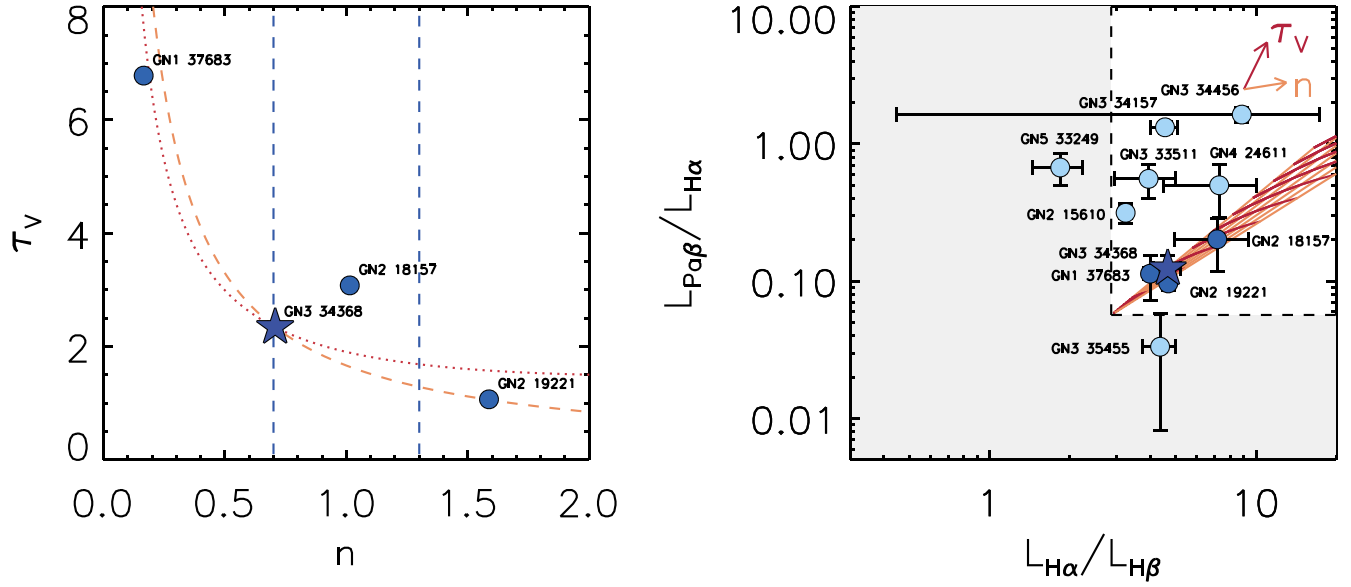


**Figure 1.** (Left) Dust-law slopes and normalizations implied by the analytic approach for galaxies with acceptable values (non-negative  $n$  and  $\tau_v$ ). For one galaxy (GN3 34368; star), we show the family of solutions from the individual  $\text{Pa}\beta/\text{H}\alpha$  (red dotted line) and  $\text{H}\alpha/\text{H}\beta$  (orange dashed line) ratios separately, with the joint solution where the two dotted lines cross. Standard dust-law slopes expected for diffuse ISM ( $n = 0.7$ ) and stellar birth clouds ( $n = 1.3$ ) are shown (light blue dashed lines; Charlot & Fall 2000). (Right) Observed emission line ratios for the 11 galaxies in the Cleri et al. (2020) sample (blue filled symbols). The expected line ratios for standard dust-law slopes (orange;  $n = 0.7$ – $1.3$ ) and a range of normalizations (red;  $\tau_v = 0.1$ – $10$ ) are shown, with the arrows indicating the direction of increasing values. The intrinsic line ratios, assuming Case B recombination, are shown with dashed black lines; two galaxies are  $\sim 1\sigma$ – $3\sigma$  outliers, with measurements lying below these values, i.e., in the “unphysical” regime (gray shaded region). The four galaxies that are well-explained by a simple power-law dust attenuation law are shown in both panels (filled dark blue symbols), with the example galaxy indicated (GN3 34368; star). Individual galaxy ID numbers are shown in both panels.

known intrinsic line ratios, and the dust-law slope  $n$ :

$$\frac{\ln[(F_{\text{H}\alpha}/F_{\text{H}\beta})/(L_{\text{H}\alpha}/L_{\text{H}\beta})]}{\ln[(F_{\text{Pa}\beta}/F_{\text{H}\alpha})/(L_{\text{Pa}\beta}/L_{\text{H}\alpha})]} = \frac{(\lambda_{\text{H}\beta}/\lambda_{\text{H}\alpha})^{-n} - 1}{1 - (\lambda_{\text{Pa}\beta}/\lambda_{\text{H}\alpha})^{-n}}. \quad (5)$$

Solving Equation (5) using Newton–Raphson iteration, we obtain  $n$ ; plugging the result back into Equations (3) and (4), we can solve for  $\tau_v$ .

As a demonstration, we apply this approach first to one of the galaxies in the CLEAR sample (GN3 34368). The measurement of the Balmer decrement yields a curve within the slope-normalization parameter space. The  $\text{Pa}\beta/\text{H}\alpha$  ratio corresponds to a second curve, and the point where the two curves cross represents the value of slope and normalization implied by the nebular lines from that galaxy. This is shown in Figure 1 (left panel).

When we apply this approach to the rest of the CLEAR sample, we find that a total of four galaxies yield physically plausible, albeit varied, dust-law slope and normalization values. In Figure 1 (left panel), we show the results for these four galaxies. For comparison, we also plot the dust-law slopes proposed by Charlot & Fall (2000), with  $n = 0.7$  representing diffuse interstellar medium (ISM) and  $n = 1.3$  representing stellar birth clouds. Hereafter, we refer to the range  $n = 0.7$ – $3$  as “standard” dust laws. Under our baseline scenario, the results in Figure 1 (left panel) seem to imply a wide range of dust laws for this small subset of galaxies.

In the rest of the galaxy sample, however, this analytic approach yields negative dust-law slopes and/or normalizations. In Figure 1 (right panel), we plot the observed emission line ratios for the entire sample, along with predictions for standard dust-law slopes and a range of normalizations. Four galaxies have line

ratios that are consistent with standard dust laws to within  $1\sigma$ , but a comparable number (five galaxies) have significant  $\text{Pa}\beta/\text{H}\alpha$  excesses. While this could in part be due to the fact that this sample was  $\text{Pa}\beta$ -selected, we note that four of these cases are more than  $3\sigma$  away from the expectations for standard dust laws. Finally, two galaxies are  $1\sigma$ – $3\sigma$  “outliers,” with observed line ratios below the intrinsic Case B values.

#### 4. Accounting for Observational Uncertainties

Assuming our baseline scenario, we can then determine the best estimate for the dust-law slope and normalization after accounting for observational uncertainties. To do this, we employed a posterior-sampling approach, equivalent to a Bayesian inference method with uniform priors. We generated a model grid, varying the slope and normalization of the dust attenuation law. Assuming the intrinsic ratios of  $\text{H}\alpha/\text{H}\beta$  and  $\text{Pa}\beta/\text{H}\alpha$  appropriate for Case B recombination, we then calculated the expected observed ratios for each combination of dust-law slope and normalization. We assumed wide uniform priors on both the slope and normalization ( $0 < n < 30$ ,  $0 < \tau_v < 30$ ). For each galaxy, we then used the observed line ratios and observational errors to compute  $\chi^2$ , and found the maximum likelihood solution implied by the grid. The likelihood contours are shown for each galaxy in Figure 2, and the implied slope and normalization corresponding to the maximum likelihood (minimum  $\chi^2$ ) is indicated.

Out of the sample, one galaxy (GN2 19221) has a well-constrained dust-law slope ( $n \sim 1.3$ ) and normalization ( $\tau_v \sim 1.0$ ). Three additional galaxies (GN1 37683, GN2 18157, GN3 34368) have solutions consistent with standard dust-law slopes (within the contour containing 68.3% of the total likelihood, given the assumed priors) and far from the assumed prior boundaries. These are the same four galaxies that yielded acceptable solutions using the simple analytic approach (Section 3). However, six galaxies show results at or near the boundary of our uniform prior ranges.

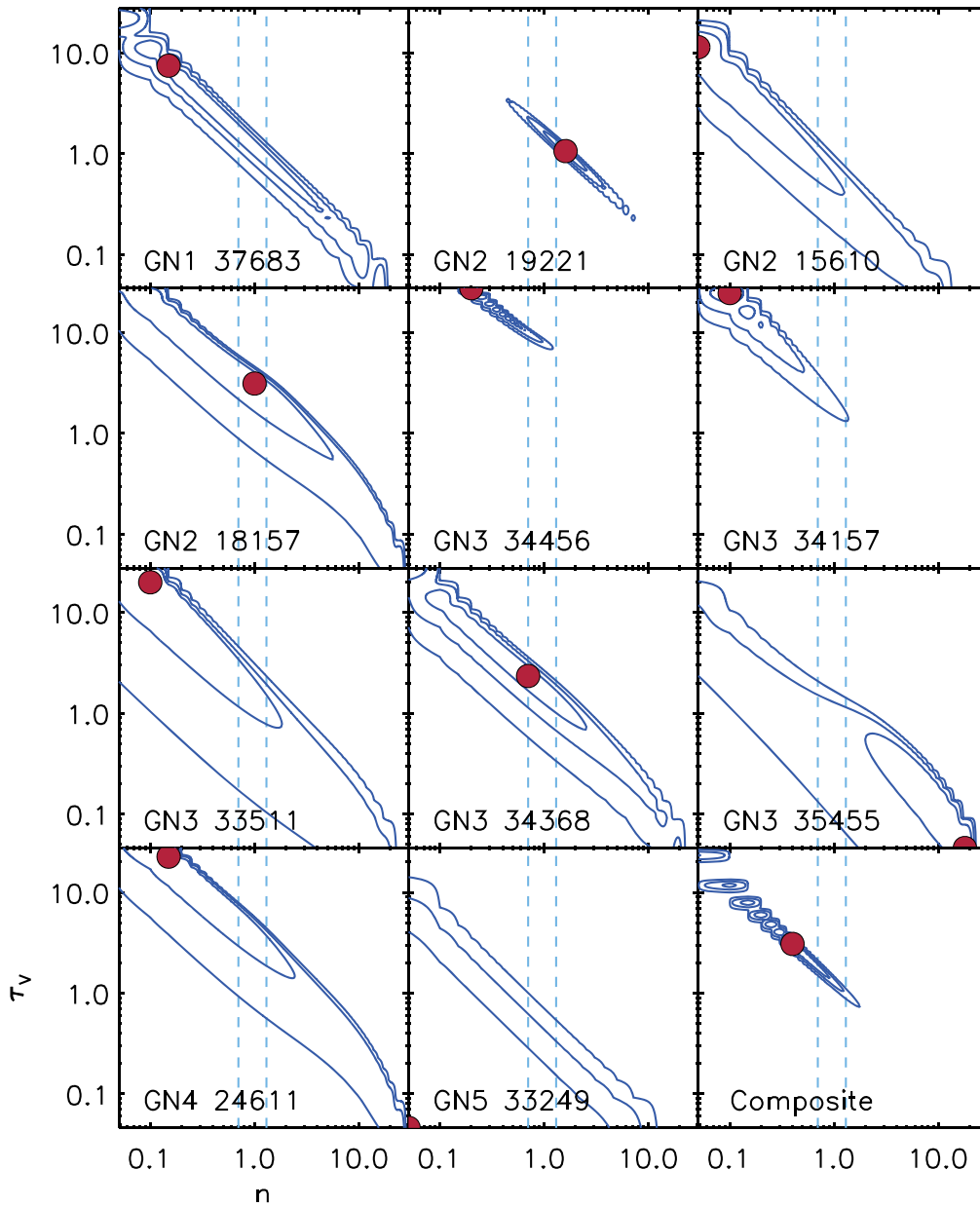


**Figure 2.** Best-fit dust-law slope ( $n$ ) and normalization ( $\tau_V$ ) accounting for observational uncertainties for each galaxy, and in the lower right panel, for a composite generated by computing the error-weighted mean and uncertainty of the full sample. Contours contain 68.3%, 95.4%, and 99.7% of the total likelihood given the assumed priors, and the corresponding location of the minimum  $\chi^2$  is shown (filled red circles). Standard dust-law slopes expected for diffuse ISM ( $n = 0.7$ ) and stellar birth clouds ( $n = 1.3$ ) are shown (light blue dashed lines; Charlot & Fall 2000). One galaxy (GN2 19221) is well-constrained with the existing data. Most of the sample overlaps standard dust-law slopes, given the current observational uncertainties, although some individual galaxies (and the full-sample composite) are more consistent with steeper or shallower dust laws.

In three of these cases (GN2 15610, GN3 33511, GN4 24611), the 68.3% confidence intervals overlap standard dust-law slopes, but for three galaxies (GN3 34456, GN3 34157, GN3 35455), one of which (GN3 34456) has the most extreme  $\text{Pa}\beta/\text{H}\alpha$  ratio of the sample, the confidence intervals are skewed toward shallower or steeper slopes. As before, for one galaxy (GN5 33249), the smallest in the sample, no acceptable solution is found. If we were to make the assumption that this sample of galaxies represents 11 independent realizations of the same underlying physical conditions, we can repeat the analysis using a composite galaxy defined by the error-weighted mean and uncertainty of the emission line ratios for the full sample. The result, shown in the lower right panel of Figure 2, implies that this galaxy sample prefers somewhat shallower-than-standard dust-law slopes. This is

consistent with the takeaway from Figure 1 (right panel), where a fair fraction of the sample showed enhanced  $\text{Pa}\beta/\text{H}\alpha$  ratios above the standard dust-law curves, i.e., in the direction of lower  $n$ . Thus, we are left with the impression that the observed emission line ratios imply a diversity of rather extreme, and in some cases unphysical, dust-law slopes across this sample of galaxies.

## 5. Influence of Astrophysical versus Observational Effects

It is possible that the baseline scenario is not accurate and that the unusual observed line ratios driving these results reflect subunity covering fractions of dusty ISM or ground-based Balmer line measurements that are either over- or undercorrected for slit



losses. In the rest of this section, we explore these two possibilities to see how well we can explain the line ratios from the observed sample.

### 5.1. Covering Fractions

One explanation for the unusual observed line ratios in certain galaxies is different covering fractions of dusty ISM (Cleri et al. 2020), such that some regions are completely opaque to the Balmer lines whereas others are much less so. In this scenario, the disk-integrated Paschen emission comes from the entire galaxy, but the Balmer lines are detected predominantly from the subset of sightlines with low dust.

To explore this effect, we make the following adjustments to the analytic calculation. We assume that lines of sight within the galaxy are either dusty or dust-free. All Paschen and Balmer line flux from the dust-free lines of sight is observed, whereas line flux from the dusty portion is attenuated according to the dust law. We define the covering fraction  $f_{\text{cov}}$  to be the fraction of the galaxy covered by dusty ISM. Thus,  $f_{\text{cov}} = 0.0$  implies that none of the galaxy experiences dust attenuation, whereas  $f_{\text{cov}} = 1.0$  means that the entire galaxy experiences dust attenuation given by  $\tau_\lambda$ , at which point the situation reduces to the baseline scenario in Section 3. We write down the observed line flux ( $F_\lambda$ ) as a function of the true line luminosity ( $L_\lambda$ ),

$$F_\lambda = [(1 - f_{\text{cov}})L_\lambda + f_{\text{cov}}L_\lambda e^{-\tau_\lambda}] \times \frac{1}{4\pi d_L^2}, \quad (6)$$

where  $\lambda$  corresponds to the wavelengths of Pa $\beta$ , H $\alpha$ , and H $\beta$ , respectively. The corresponding line ratios are therefore

$$\frac{F_{\text{Pa}\beta}/F_{\text{H}\alpha}}{L_{\text{Pa}\beta}/L_{\text{H}\alpha}} = \frac{(1 - f_{\text{cov}}) + f_{\text{cov}} e^{-\tau_V(\lambda_{\text{Pa}\beta}/5500 \text{ \AA})^{-n}}}{(1 - f_{\text{cov}}) + f_{\text{cov}} e^{-\tau_V(\lambda_{\text{H}\alpha}/5500 \text{ \AA})^{-n}}} \quad (7)$$

$$\frac{F_{\text{H}\alpha}/F_{\text{H}\beta}}{L_{\text{H}\alpha}/L_{\text{H}\beta}} = \frac{(1 - f_{\text{cov}}) + f_{\text{cov}} e^{-\tau_V(\lambda_{\text{H}\alpha}/5500 \text{ \AA})^{-n}}}{(1 - f_{\text{cov}}) + f_{\text{cov}} e^{-\tau_V(\lambda_{\text{H}\beta}/5500 \text{ \AA})^{-n}}}. \quad (8)$$

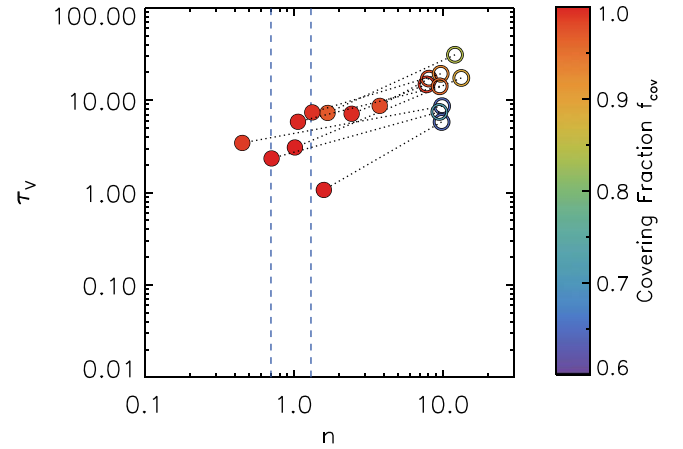
Thus far, we have not imposed any restrictions on the analysis, other than that the dust-law slope and normalization must be non-negative. In practice, however, large attenuation of the Balmer lines would imply very large, and potentially implausible, star formation rates. The measured star formation rates from Cleri et al. (2020) are all  $\lesssim 2 M_\odot \text{ yr}^{-1}$  based on the observed ultraviolet and infrared luminosities. Therefore, we impose a conservative upper limit on the implied star formation rate of  $10 M_\odot \text{ yr}^{-1}$ . We solve Equations (7) and (8) and determine the range of covering fractions for which such “acceptable” solutions exist (i.e., a non-negative dust-law normalization and slope, and an implied dust-corrected star formation rate of  $< 10 M_\odot \text{ yr}^{-1}$ ).

Table 1 lists the derived minimum and maximum covering fractions for the galaxy sample. For two galaxies, there is no acceptable solution. This is not surprising, as these two galaxies are the known outliers, with observed line ratios in the “unphysical” regime (Figure 1, right panel). In Figure 3, we show the range of covering fractions that produce acceptable results for each of the other nine galaxies. Allowing for a sub-unity covering fraction can explain the line ratios for the rest of the sample, with the lowest allowed covering fractions being 64%–99% and the highest allowed covering fractions being 97%–100%. However, in each galaxy, a lower covering fraction implies a steeper dust-law slope and higher normalization. Since substantially sub-unity covering fractions would imply very

**Table 1**  
Dust Covering Fractions

Field	ID	$f_{\text{cov,min}}$	$f_{\text{cov,max}}$
GN1	37683	0.64	0.99
GN2	19221	0.64	1.00
GN2	15610	0.84	0.97
GN2	18157	0.89	1.00
GN3	34456	0.99	1.00
GN3	34157	0.97	0.98
GN3	33511	0.93	0.99
GN3	34368	0.72	1.00
GN3	35455	...	...
GN4	24611	0.96	1.00
GN5	33249	...	...

**Note.** These are the minimum and maximum allowed dust covering fractions that lead to non-negative dust-law slopes  $n$  and normalizations  $\tau_V$ , and a star formation rate of  $\text{SFR} < 10 M_\odot \text{ yr}^{-1}$ .



**Figure 3.** Range of covering fractions ( $f_{\text{cov}}$ , indicated with the color bar) that produce acceptable results from the analytic approach (Equations (7) and (8)). Dotted lines connect the minimum (open circle) and maximum (filled circle) covering fraction allowed for each galaxy. Standard dust-law slopes expected for diffuse ISM ( $n = 0.7$ ) and stellar birth clouds ( $n = 1.3$ ) are shown (light blue dashed lines; Charlot & Fall 2000). While allowing for  $f_{\text{cov}} < 1$  permits an acceptable solution for 9/11 galaxies in the sample, substantially sub-unity covering fractions imply very extreme dust-law slopes ( $n > 1.3$ ). For standard dust-law slopes, high but in some cases sub-unity covering fractions ( $0.97 < f_{\text{cov}} < 1$ ) are indicated.

extreme dust laws, they are therefore not the preferred explanation for the line ratios in this sample. For standard dust law slopes, high but in some cases sub-unity covering fractions ( $\gtrsim 97\%$ ) are required by our analysis.

### 5.2. Slit Loss Correction Underestimates

On the other hand, observational biases may be driving the unusual line ratios within the sample. While the Pa $\beta$  measurements represent disk-integrated values, the H $\alpha$  and H $\beta$  fluxes were derived using a spectroscopic slit and were then corrected for both throughput and slit losses as described in Section 2. However, this correction assumed that there was no difference in equivalent width between regions inside and outside of the slit. While this assumption was reasonable on average given a typical galaxy size of  $r_{\text{eff}} < 0''.95$  (Weiner et al. 2007), it may be violated in galaxies that are large compared to the size of the slit or with line emission that is offset or more extended than the continuum. The resulting variable equivalent

**Table 2**  
Empirical Slit Losses

Field	ID	$r_{\text{eff}}^a$ (arcsec)	Slit Loss (best case)	Slit Loss (worst case)
GN1	37683	0.69	0.01	0.36
GN2	19221	0.60	0.27	0.37
GN2	15610	1.49	0.45	0.68
GN2	18157	1.20	0.09	0.56
GN3	34456	1.10	0.32	0.56
GN3	34157	1.10	0.49	0.60
GN3	33511	0.60	0.00	0.27
GN3	34368	0.30	0.13	0.22
GN3	35455	0.22	0.00	0.03
GN4	24611	1.30	0.37	0.60
GN5	33249	0.20	0.01	0.02

**Notes.** Empirical best (worst) case slit losses represent the most (least) likely slit loss corrections applied to the tabulated Balmer fluxes. These were estimated using the observed stellar continuum morphology of each galaxy, the slit orientation, and the assumption that nebular and stellar continuum morphologies are equal, as described in the text.

<sup>a</sup> Effective radii ( $r_{\text{eff}}$ ) are taken from van der Wel et al. (2012).

width could lead to larger slit losses for line emission than for continuum. In that case, the assumption of constant equivalent width across the galaxy would result in an underestimate of the emission line slit loss correction for the Balmer line fluxes, and as a result, a measured  $\text{Pa}\beta/\text{H}\alpha$  enhancement. Figure 1 (right panel) shows that at least half of the galaxy sample have a  $\text{Pa}\beta/\text{H}\alpha$  enhancement that cannot be explained by acceptable dust laws; therefore, it seems plausible that the assumption of constant equivalent width versus position may not be valid for some of these galaxies.

To assess the relative importance of slit losses, we empirically estimated the effective slit loss correction that was applied previously (as described in Section 2) using the known size and morphology of the galaxy (van der Wel et al. 2012) and the width of the spectroscopic slit employed in the ground-based observations (1"; Wirth et al. 2004). One complication is that while the ground-based observations used a Keck/DEIMOS multislit mask at a particular position angle, the individual slitlets were milled at an orientation within  $\pm 30^\circ$  of that angle. Although the stated goal was to align the slit with the major axis of the galaxy, when possible, the resulting position angle of the Keck/DEIMOS slitlets relative to each galaxy's major axis is not specified. We therefore computed the slit losses for both the best (and more likely) case, with the slitlet fully aligned with the galaxy major axis resulting in minimal slit losses, and the worst case, with the slitlet perpendicular to the galaxy major axis resulting in maximal slit losses. In all cases, we assumed the galaxy was centered in the slitlet. While these empirical slit loss corrections could be underestimated—for example, in galaxies that depart from a single Sérsic profile due to strong dust lanes—they nonetheless provide an indication of which galaxies will be most susceptible to errors in the slit loss correction.

The empirically estimated slit losses, along with the tabulated  $r_{\text{eff}}$  values (van der Wel et al. 2012), are given in Table 2. In the best case, the slit losses were between 0% and 49%, while in the worst case they ranged from 2% to 68%. Some galaxies are small compared to the slit (at least as measured by continuum  $r_{\text{eff}}$ ), resulting in minimal empirical slit loss corrections. Interestingly, both of the two outlier galaxies had essentially no slit losses, due to their small effective radii ( $r_{\text{eff}} \sim 0''.2$ ). On the other hand, five of the galaxies are large

compared to the slit, resulting in large ( $>50\%$ , in the worst case) empirical slit loss corrections. This suggests that variable equivalent width or line emission that is more extended than or offset from the continuum could plausibly have led to an underestimate in the slit loss correction in these cases.

To further explore the possibility of over- or underestimated slit loss corrections in this sample, we make the following adjustments to the analytic calculation. We use  $f_{\text{slit}}$  as a factor that accounts for any additional uncorrected slit losses, with a range from  $-0.99$  to  $0.99$ . Physically, a negative value of  $f_{\text{slit}}$  corresponds to the situation where the emission line equivalent width is smaller outside the slit than inside, resulting in a previous overcorrection, whereas a positive  $f_{\text{slit}}$  means the line equivalent width is larger outside the slit, leading the previous correction to be underestimated. We then write down the tabulated line flux ( $F_\lambda$ , including the nominal slit loss correction) as a function of the true line luminosity ( $L_\lambda$ , fully slit-loss-corrected) for the two Balmer lines:

$$F_{\text{H}\alpha} = L_{\text{H}\alpha} e^{-\tau_V(\lambda_{\text{H}\alpha}/5500 \text{ \AA})^{-n}} \times \frac{(1 - f_{\text{slit}})}{4\pi d_L^2} \quad (9)$$

$$F_{\text{H}\beta} = L_{\text{H}\beta} e^{-\tau_V(\lambda_{\text{H}\beta}/5500 \text{ \AA})^{-n}} \times \frac{(1 - f_{\text{slit}})}{4\pi d_L^2}. \quad (10)$$

We continue to use Equation (2) for  $\text{Pa}\beta$ , as the disk-integrated slitless grism measurements are unaffected by slit losses.

The corresponding  $\text{Pa}\beta/\text{H}\alpha$  line ratio is therefore:

$$\frac{F_{\text{Pa}\beta}/F_{\text{H}\alpha}}{L_{\text{Pa}\beta}/L_{\text{H}\alpha}} = \frac{e^{-\tau_V[(\lambda_{\text{Pa}\beta}/5500 \text{ \AA})^{-n} + (\lambda_{\text{H}\alpha}/5500 \text{ \AA})^{-n}]}}{(1 - f_{\text{slit}})}. \quad (11)$$

The  $\text{H}\alpha/\text{H}\beta$  ratio is still given by Equation (4), as the slit losses are assumed to be the same and therefore cancel out for the two Balmer lines.

We then calculate what range of  $f_{\text{slit}}$  values would be required in order to produce an acceptable solution. As before, we require non-negative  $n$  and  $\tau_V$ , and impose a limit on the implied star formation rate of  $10 M_\odot \text{ yr}^{-1}$ . The results are shown in Figure 4 and in Table 3, along with the estimated stellar masses from Skelton et al. (2014). One of the outlier galaxies (GN5 33249) returned unphysical results, as before; this is not surprising, as the  $\text{H}\alpha/\text{H}\beta$  ratio for this galaxy is below the Case B intrinsic value, so there is no slit loss correction that can bring it into the physical regime. The other outlier galaxy (GN3 35455) can be explained but only in the case of a high slit loss correction overestimate ( $f_{\text{slit}} < -0.71$ ), which is implausible given its small physical size ( $r_{\text{eff}} \sim 0''.22$ ). The remaining nine galaxies show a range of additional slit loss corrections. In three cases, allowable  $f_{\text{slit}}$  values can be either positive or negative, whereas in six cases, only  $f_{\text{slit}} > 0$  (a slit loss correction underestimate) is permitted. Correcting for such slit loss underestimates generically reduces the  $\text{Pa}\beta/\text{H}\alpha$  flux ratio toward the intrinsic Case B value without modifying the Balmer decrement, changing the best-fit slope and normalization. Thus, correcting for slit losses that may have been moderately over- or underestimated previously may bring most, although not all, of the galaxy sample into agreement with standard dust laws.

## 6. Discussion

Using an analytic approach, we showed that 4 of the 11 galaxies are consistent with a simple power-law dust attenuation

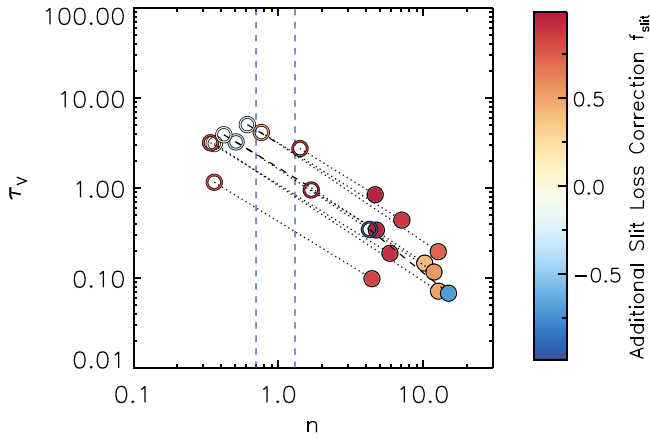


**Figure 4.** Range of allowed additional slit loss corrections ( $f_{\text{slit}}$ , indicated with the color bar) that produce acceptable results, i.e., non-negative  $n$  and  $\tau_V$  with  $\text{SFR} < 10 M_{\odot} \text{ yr}^{-1}$ , from the analytic approach (Equations (4) and (11)). Dashed and dotted lines connect the minimum (open) and maximum (filled)  $f_{\text{slit}}$  values for each galaxy, where dashed lines indicate negative  $f_{\text{slit}}$  values (a previous overcorrection) and dotted lines indicate positive  $f_{\text{slit}}$  values (a previous undercorrection). Standard dust-law slopes expected for diffuse ISM ( $n = 0.7$ ) and stellar birth clouds ( $n = 1.3$ ) are shown (light blue dashed lines; Charlot & Fall 2000). Moderate slit loss over- or undercorrection may be present in the tabulated Balmer fluxes, assuming that standard dust laws apply.

**Table 3**  
Additional Allowed Slit Loss Correction

Field	ID	$\log M_{*}^a$ ( $M_{\odot}$ )	$f_{\text{slit,min}}$	$f_{\text{slit,max}}$
GN1	37683	8.61	0.06	0.49
GN2	19221	9.05	-0.40	0.40
GN2	15610	9.43	0.77	0.81
GN2	18157	8.96	-0.30	0.71
GN3	34456	10.01	0.87	0.95
GN3	34157	9.23	0.93	0.95
GN3	33511	8.63	0.81	0.89
GN3	34368	8.47	-0.12	0.53
GN3	35455	7.69	-0.99	-0.71
GN4	24611	8.91	0.51	0.87
GN5	33249	7.67	...	...

**Notes.** These are the minimum and maximum allowed  $f_{\text{slit}}$  values (implying a previous slit loss correction overestimate if negative or underestimate if positive) that lead to non-negative dust-law slopes  $n$  and normalizations  $\tau_V$ , and a star formation rate of  $\text{SFR} < 10 M_{\odot} \text{ yr}^{-1}$ .

<sup>a</sup> Stellar masses are taken from Skelton et al. (2014).

law. However, the required slopes ( $n$ ) ranged from much flatter than expected for the diffuse ISM ( $n = 0.7$ ) to much steeper than expected for stellar birth clouds ( $n = 1.3$ ). A closer look revealed that the remaining seven galaxies have unusual line ratios that are far from the predicted locus using standard dust-law slopes. While the current sample of galaxies may be biased toward higher  $\text{Pa}\beta/\text{H}\alpha$  and lower  $\text{H}\alpha/\text{H}\beta$  ratios due to the fact that it was selected by requiring detections in  $\text{Pa}\beta$ ,  $\text{H}\alpha$ , and  $\text{H}\beta$  (Cleri et al. 2020), it nonetheless provides a useful opportunity to explore the physical interpretation of these more extreme line ratios.

### 6.1. Astrophysical and Observational Considerations

Cleri et al. (2020) discussed the possibility that these unusual line ratios are the result of sub-unity covering fractions of dusty ISM. This might occur, for example, if a galaxy has a prominent dust lane (Cleri et al. 2020) or a collimated, dusty outflow (e.g.,

Walter et al. 2002). In this case, relatively dust-free lines of sight would contribute Paschen-to-Balmer line ratios close to their intrinsic Case B values, but dusty lines of sight would show highly attenuated Balmer relative to Paschen emission, creating an enhancement of the overall observed Paschen-to-Balmer line ratio.

Our analysis has suggested that sub-unity covering fractions could plausibly explain the extreme  $\text{Pa}\beta/\text{H}\alpha$  line ratios in at least some of the galaxy sample. To further explore how this works, in Figure 5, we show the resultant line ratios for four different covering fractions  $f_{\text{cov}}$ , along with the observed line ratios for the galaxy sample. In each panel, we assume a different dust attenuation law slope  $n$ , ranging from shallower ( $n = 0.5$ ) to steeper ( $n = 2.0$ ) than the standard range ( $n = 0.7$ – $1.3$ ). The resultant curves correspond to a range of dust-law normalizations ( $0 < \tau_V < 30$ ), with the direction of increasing  $\tau_V$  indicated with an arrow in the bottom right-hand panel. With a unity covering fraction, the line ratios increase with normalization, as higher dust column leads to progressively greater attenuation of the shorter-wavelength  $\text{H}\alpha$  and  $\text{H}\beta$  emission lines. For slightly sub-unity covering fractions ( $f_{\text{cov}} \gtrsim 0.9$ ), however, the curves form loops in the line ratio diagram. This comes about because, at sufficient dust columns, the few lines of sight that are dust-free start to dominate the observed flux, causing the observed line ratios to converge back toward the intrinsic Case B values. The dust-law normalization where this occurs, however, depends on the line ratio, with the shorter wavelength  $\text{H}\alpha/\text{H}\beta$  ratio beginning to return to intrinsic values at lower dust columns than the longer wavelength  $\text{Pa}\beta/\text{H}\alpha$  ratio. This can be seen in Figure 6, where for non-unity covering fractions, the line ratios initially increase as a function of dust-law normalization, but then decrease again past a critical value, with the  $\text{Pa}\beta/\text{H}\alpha$  ratio turning over at higher normalizations than the  $\text{H}\alpha/\text{H}\beta$  ratio. We note that this effect occurs only for very high but non-unity covering fractions; at  $f_{\text{cov}} \lesssim 0.9$ , the larger fraction of dust-free lines of sight causes the observed line ratios to remain close to their intrinsic Case B values. Thus, sub-unity covering fractions do seem to be a plausible explanation for most of the unusual line ratios observed in this sample. We note that a high or even unity covering fraction is favored for the galaxy with the most extreme  $\text{Pa}\beta/\text{H}\alpha$  ratio (GN3 34456), which shows a clear dust lane in the existing GOODS-N and CANDELS imaging. Future measurements with more than three emission lines will allow for independent constraints on the covering fraction of dusty ISM in galaxies.

A second possibility was that underestimates in ground-based slit loss corrections suppressed the measured Balmer line emission, which, when compared with space-based full-galaxy  $\text{Pa}\beta$  measurements, resulted in an enhancement of the observed  $\text{Pa}\beta/\text{H}\alpha$  line ratio. In exploring this possibility further, we found that a range of additional slit loss corrections ( $f_{\text{slit}}$ ) are allowed by the data. In particular, for 3 out of the 11 galaxies, the allowed range straddled  $f_{\text{slit}} = 0$  and standard dust-law slopes, suggesting that the applied slit loss corrections were likely correct. For six of the galaxies, however, additional slit loss corrections of at least 6%–93%, depending on the galaxy, were required in order for the line ratios to be consistent with acceptable dust-law parameters.

Since the nominal slit loss correction described in Section 2 assumed a constant emission line equivalent width across the galaxy (both inside and outside the slit), deviations from this assumption would lead to errors in the resulting flux ratios. This would be the case if the line emission is more or less extended than the continuum emission from the galaxy.

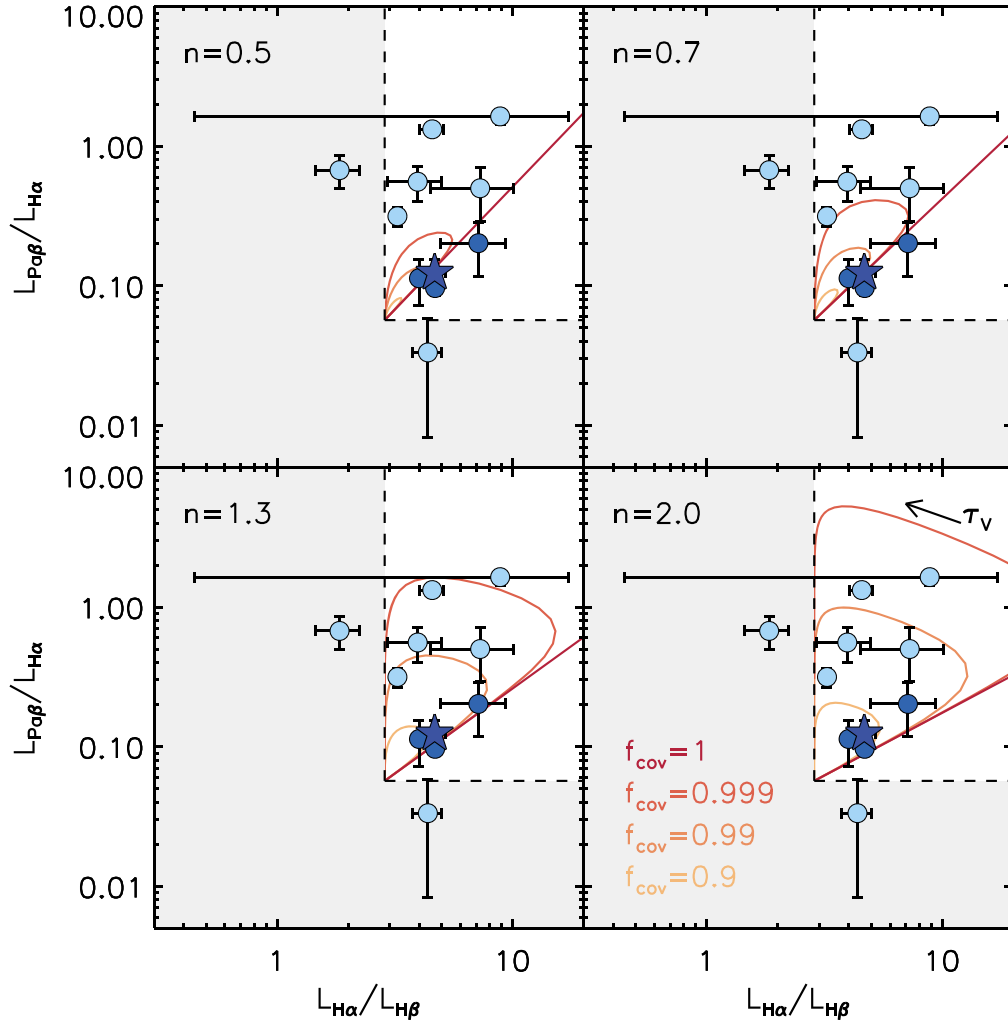


**Figure 5.** Effect of covering fraction ( $f_{\text{cov}}$ ) on the  $\text{Pa}\beta/\text{H}\alpha$  vs.  $\text{H}\alpha/\text{H}\beta$  line ratios (orange/red lines), for a different value of the dust attenuation law slope ( $n$ ) in each panel. The direction of increasing dust attenuation law normalization ( $\tau_v$ ) is indicated with an arrow in the lower right ( $n = 2.0$ ) panel. For comparison, the observed emission line ratios for the 11 galaxies in the Cleri et al. (2020) sample are shown as in Figure 1 (blue filled symbols). The intrinsic line ratios, assuming Case B recombination, are shown with dashed black lines, with the “unphysical” regime indicated (gray shaded region). Slightly sub-unity covering fractions ( $f_{\text{cov}} \gtrsim 0.9$ ) lead to extreme line ratios, similar to what is seen in the galaxy sample. However, for substantially sub-unity covering fractions ( $f_{\text{cov}} \lesssim 0.9$ ) the emission line ratios return to the Case B intrinsic values, due to the higher fraction of unattenuated sightlines.

Indications from the 3D-HST survey are that this is the case at  $z \sim 1$ , with  $\text{H}\alpha$  emission being somewhat more extended than the  $R$ -band continuum (Nelson et al. 2012, 2013). In addition, recent results from the CLEAR survey suggest that the relative compactness of the line and continuum emission may correlate with galaxy mass (J. Matharu et al. 2022, in preparation). Specifically, for galaxies less massive than  $\log(M_*/M_\odot) \sim 9.2$  (8/11 galaxies in the current sample), the  $\text{H}\alpha$  emission appears to be comparable to or more compact on average than the continuum, which would lead to a slit loss overestimate (negative  $f_{\text{slit}}$ ). The applicability of this result to our galaxy sample is unclear, for while this subset includes the three galaxies with negative allowed  $f_{\text{slit}}$ , it also includes two galaxies for which only large positive  $f_{\text{slit}}$  values are allowed. On the other hand, three galaxies in the sample are more massive than  $\log(M_*/M_\odot) \sim 9.2$ , where there is evidence that  $\text{H}\alpha$  emission will on average be more extended than the continuum. In this case, one would expect the slit loss correction to be underestimated (positive  $f_{\text{slit}}$ ), leading to enhanced  $\text{Pa}\beta/\text{H}\alpha$  ratios. Indeed, all three of these more massive galaxies require large positive  $f_{\text{slit}}$  values, and intriguingly, two of them (GN3

34456, GN3 34157) represent the highest two  $\text{Pa}\beta/\text{H}\alpha$  ratios in the sample. Thus, while it is difficult to draw strong conclusions, it appears that variations in equivalent width across the galaxy, and the resulting underestimated slit loss corrections, could explain some of the most enhanced  $\text{Pa}\beta/\text{H}\alpha$  line ratios.

Clearly, it would be best to circumvent these issues by removing the need for slit loss corrections altogether. This could be done either by using disk-integrated Balmer line fluxes from narrowband imaging (requiring a correction for  $[\text{N II}]$  in the case of  $\text{H}\alpha$ ), integral field spectroscopy (IFS), or slitless grism observations, or by obtaining all three line measurements with a consistent spectroscopic slit from space or with appropriate correction for atmospheric dispersion. In addition, high signal-to-noise constraints on all three lines will be important for deriving meaningful constraints on the dust-law normalization and slope. From the existing data on this sample, one galaxy (GN2 19221) is in that position, where the effects of sub-unity covering fraction are likely negligible, the slit losses are accounted for plausibly well, and the observational uncertainties are small enough that the galaxy is



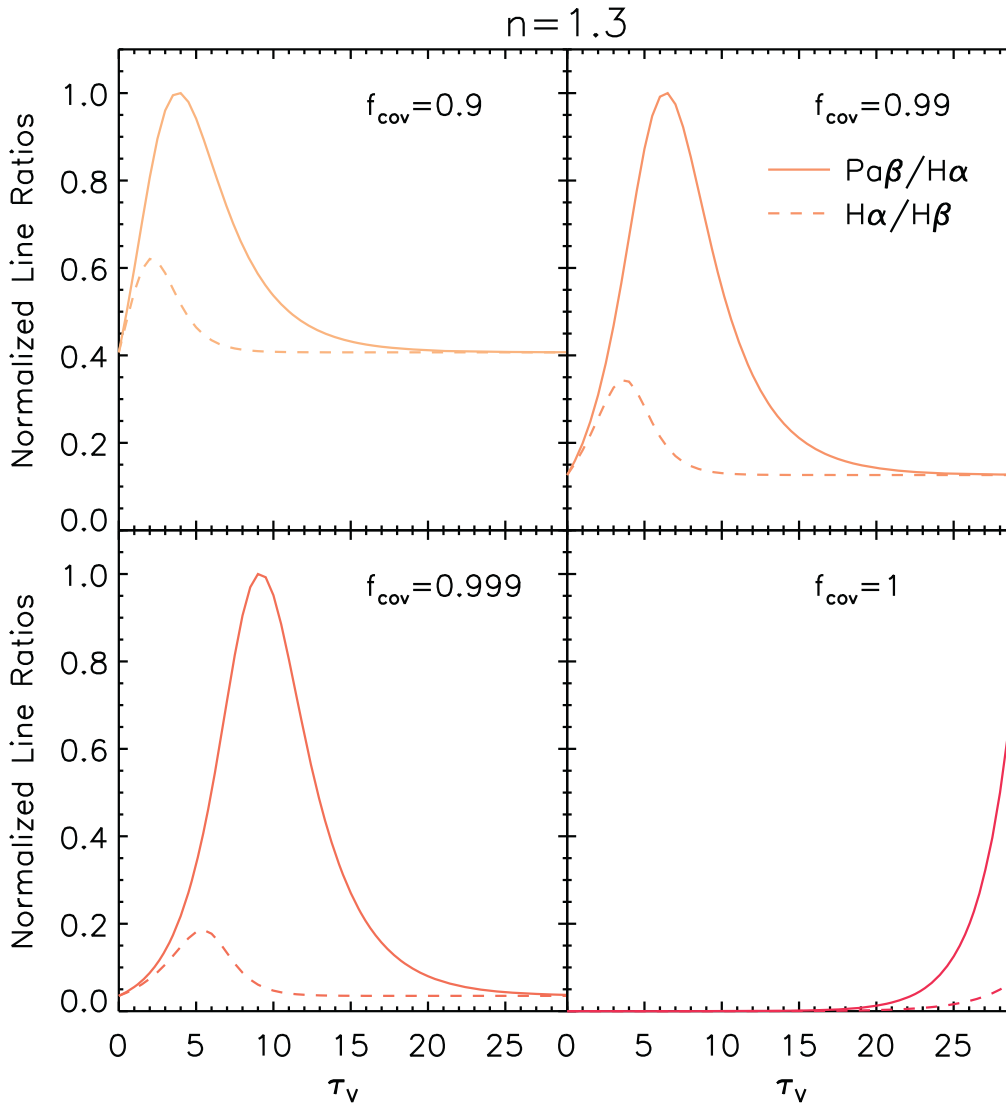


**Figure 6.** Normalized line ratios as a function of dust attenuation law normalization ( $\tau_V$ ), for different values of covering fraction ( $f_{\text{cov}}$ ).  $\text{Pa}\beta/\text{H}\alpha$  and  $\text{H}\alpha/\text{H}\beta$  ratios are shown as solid and dashed lines, respectively. For slightly sub-unity covering fractions ( $f_{\text{cov}} \gtrsim 0.9$ ), both line ratios increase with increasing dust attenuation up to a certain maximum value, after which they decline back to their intrinsic values. However, the shorter wavelength pair,  $\text{H}\alpha/\text{H}\beta$ , reaches its peak ratio at lower dust attenuation than  $\text{Pa}\beta/\text{H}\alpha$ . Thus, slightly sub-unity covering fractions combined with moderate-to-high dust attenuation can lead to unusually high  $\text{Pa}\beta/\text{H}\alpha$  ratios, as seen in the observed sample.

constrained to have  $n \sim 1.3$  and  $\tau_V \sim 1$ . This galaxy therefore provides a promising example of what will be possible in the near future.

### 6.2. Galaxy Morphologies

It is natural to wonder whether the morphologies across the sample can explain some of the variation in recovered dust-law parameters. To explore this, Figure 7 replicates the  $\text{Pa}\beta/\text{H}\alpha$  versus  $\text{H}\alpha/\text{H}\beta$  line ratio plot, but with each galaxy indicated using its composite CANDELS *iYH*-band imaging. However, no clear trends emerge. The four galaxies most consistent with standard dust-law slopes (GN2 19221, GN1 37683, GN2 18157, and GN3 34368) show a range of morphologies with examples of knotty star-forming disks (GB2 19221, GB3 34368), one edge-on galaxy (GB2 18157), and one that resembles a “chain” galaxy (GN1 37683). The effective radii for this subset vary widely ( $r_{\text{eff}} = 0''.3\text{--}1''.20$ ; see Table 2). For the six galaxies at or near prior boundaries and the one with no solution, the morphologies also span a broad range, including knotty

star-forming disks (GN2 15610, GN4 24611, and GN3 34157), two that are very compact (GN5 33249 and GN3 35455), and two edge-on systems (GN3 33511 and GN3 34456), with the latter showing a particularly prominent dust lane. The effective radii span a similarly broad range ( $r_{\text{eff}} = 0''.2\text{--}1''.49$ ). Thus, galaxy morphology is not obviously correlated with the dust-law constraints within this sample.

### 6.3. Nonuniversal Dust Laws

In the existing analysis, we found that some galaxies are in agreement with standard dust laws, within the broad confidence intervals. In other cases, the solutions are skewed to steeper or shallower dust-law slopes, and when treating the entire sample as a single composite galaxy, we found a preference for shallower dust-law slopes. Thus, taking the results from our relatively small sample of galaxies at face value, we see tentative evidence for a variety of dust laws in galaxies at  $z \sim 0.2$ . This would not be entirely surprising. Even in the local universe, we see ample indications of variations, with the Milky Way dust attenuation

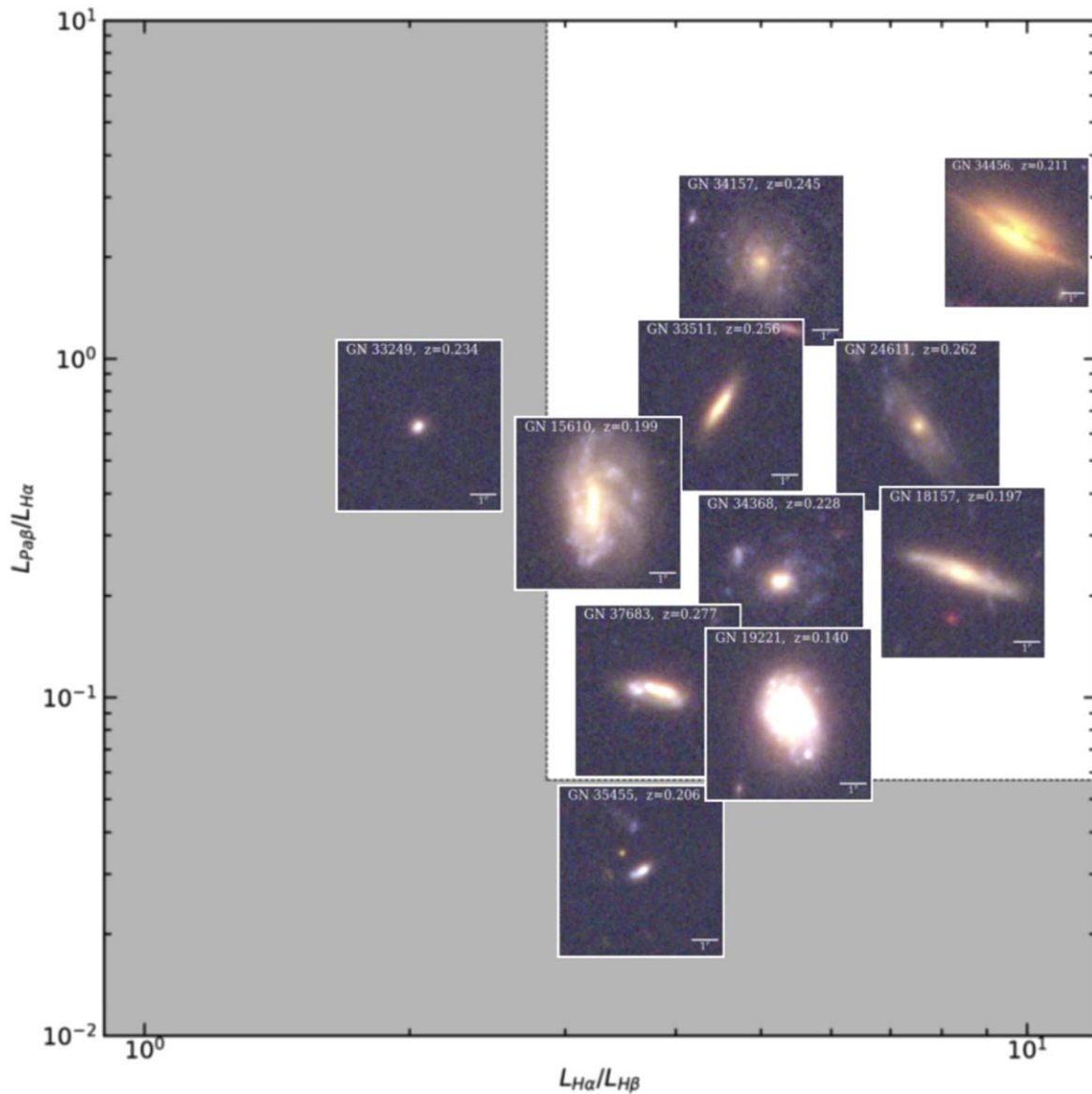


**Figure 7.** Observed  $\text{Pa}\beta/\text{H}\alpha$  and  $\text{H}\alpha/\text{H}\beta$  ratios for the 11 galaxies in the Cleri et al. (2020) sample, as shown in Figure 1 (right), but here indicated with *iYH*-band composite images. The intrinsic Case B recombination line ratios are shown as dotted black lines. The sample includes a diverse range of galaxy morphologies but no obvious trends with line ratios. The highest  $\text{Pa}\beta/\text{H}\alpha$  ratio in the sample, GN 34456, shows a significant dust lane through its center.

curve differing substantially in shape from those of the neighboring Large and Small Magellanic Clouds (LMC and SMC; e.g., Pei 1992; Gordon et al. 2003). At higher redshifts ( $z \sim 0.5\text{--}3$ ), SED-fitting approaches have presented evidence for the nonuniversality of the dust law in galaxies (Kriek & Conroy 2013; Salmon et al. 2016). This is perhaps to be expected, as the dust extinction law will reflect the dust composition and the grain size distribution, which will in turn reflect the dust production processes in the galaxy. Moreover, the geometry of the ISM can lead to different emergent dust attenuation curves in the optical and near-infrared even if the intrinsic extinction curves are the same, implying that attenuation curves are not uniquely determined even if the stellar mass, star formation rate, and metallicity are known (Narayanan et al. 2018).

We have shown that constraining dust laws using more than two emission lines can, in principle, provide a nearly model-independent, complementary way to study the intrinsic variability in dust attenuation law parameters. In doing so, we have used the

assumption of a power-law dust law. This was a simplification, but it was useful for exploring the three-line method along with various astrophysical and observational challenges. However, in reality the dust law will have a more complicated shape and potentially additional features, e.g., the 2175 Å bump. It is possible that some of the other galaxies in the sample could be explained better by a different dust law. Therefore, it would be beneficial to further investigate the detailed shape of the nebular dust law once more emission line constraints are available for a larger sample of galaxies.

#### 6.4. Leveraging the Three-line Approach

This work motivates a number of additional investigations to leverage the potential power of multiple emission lines to put constraints on the shape of the dust law in galaxies. In the local universe,  $\text{Pa}\beta$  measurements from HST already exist for a few galaxies (e.g., NGC 5194 and NGC 6946; Kessler et al. 1919). Narrowband imaging—or even better, IFS observations—of

these galaxies could be used to study the dust law in individual apertures across the galaxy disks, while disk-integrated measurements could be compared with those derived at higher redshifts.

Even more exciting is the prospect of using the James Webb Space Telescope (JWST) to follow up order-of-magnitude larger samples of intermediate- to high-redshift galaxies ( $z \approx 0.3\text{--}2$ ), where at least three nebular lines can be observed using identical NIRSpec Microshutter Array (MSA) slitlets, the NIRSpec IFU, or the NIRISS and NIRCams grisms, removing the issue of differential slit losses between key lines. Using deeper near-infrared constraints on Paschen lines from JWST and a proper treatment of upper limits, we can obtain more representative and largely model-independent constraints on the slope and normalization of the dust law of galaxies at the peak of cosmic star formation.

## 7. Conclusions


In this paper, we explored both the power of and practical challenges associated with using three hydrogen emission lines to constrain not just the normalization but also the slope of the dust attenuation law. Using a sample of 11 galaxies with existing  $H\alpha$ ,  $H\beta$ , and  $Pa\beta$  measurements, and accounting for observational uncertainties, we showed that the dust-law slope and normalization of one galaxy are well-constrained, an indication of what will be possible in future work. Eight of the other 10 galaxies can be explained using a simple power-law dust attenuation curve given current observational uncertainties, although some prefer dust-law slopes that are significantly steeper or shallower than expected from theoretical arguments. This may suggest that low-mass, low-redshift galaxies have a diversity of dust laws, reminiscent of the claims of varying dust laws in the higher-redshift universe. However, we then explored other astrophysical or observational biases that may influence the derived results. Using an analytic approach, we showed that high but sub-unity ( $>97\%$ ) covering fractions of dusty ISM can explain some of the unusual ratios seen in this sample of galaxies, but that different slit loss corrections between key lines may also be contributing to the results. This work therefore emphasizes how the three-line approach can provide important complementary constraints on the shape of the dust attenuation law, but that a naive implementation can overlook potentially serious systematic uncertainties. With deeper measurements and a consistent observational setup across all emission lines, we can hope to constrain the slope and normalization of the dust attenuation law, and potentially, with additional recombination line constraints, the dust covering fraction in individual galaxies. This in turn will improve measurements of key galaxy properties including gas-phase metallicities, ionization parameters, and instantaneous star formation rates.

The authors would like to thank Ben Weiner, Jasleen Matharu, and Sydney Lower for helpful discussions, and the anonymous referee for useful suggestions that substantially improved the quality of this paper. Figures 1–6 were created using color-blind-friendly IDL color tables developed by Paul

Tol (<https://personal.sron.nl/pault/>). M.K.M.P. acknowledges support from NSF grant AAG-1813016, and K.M.F. acknowledges support from NSF grant AAG-2006550. N.J.C. and J.R.T. acknowledge support from NSF grant CAREER-1945546 and NASA grant JWST-ERS-01345.

This work is based on data obtained for the CLEAR program (GO-14227), the 3D-HST Treasury Program (GO 12177 and 12328), and the CANDELS Multi-Cycle Treasury Program by the NASA/ESA Hubble Space Telescope, which is operated by the Association of Universities for Research in Astronomy, Incorporated, under NASA contract NAS5-26555.

## ORCID iDs

Moire K. M. Prescott  <https://orcid.org/0000-0001-8302-0565>  
 Kristian M. Finlator  <https://orcid.org/0000-0002-0496-1656>  
 Nikko J. Cleri  <https://orcid.org/0000-0001-7151-009X>  
 Jonathan R. Trump  <https://orcid.org/0000-0002-1410-0470>  
 Casey Papovich  <https://orcid.org/0000-0001-7503-8482>

## References

- Alonso-Herrero, A., Rieke, G. H., Rieke, M. J., et al. 2006, *ApJ*, 650, 835
- Boquien, M., Burgarella, D., Roehlly, Y., et al. 2019, *A&A*, 622, 103
- Calzetti, D. 1997, *AIPC*, 408, 403
- Brammer, G., van Dokkum, P. G., Franx, M., et al. 2012, *ApJS*, 200, 13
- Calzetti, D. 2001, *PASP*, 113, 1449
- Calzetti, D., Armus, L., Bohlin, R. C., et al. 1999, *ApJ*, 533, 682
- Calzetti, D., Kennicutt, R. C., Engelbracht, C. W., et al. 2007, *ApJ*, 666, 870
- Cardelli, J. A., Clayton, G. C., & Mathis, J. S. 1989, *ApJ*, 345, 245
- Charlot, S., & Fall, S. M. 2000, *ApJ*, 539, 718
- Cleri, N. J., Trump, J. R., Backhaus, B. E., et al. 2020, *arXiv:2009.00617*
- Estrada-Carpenter, V., Papovich, C., Momcheva, I., et al. 2019, *ApJ*, 870, 133
- Finkelstein, K. D., Papovich, C., Finkelstein, S. L., et al. 2011, *ApJ*, 742, 108
- Giavalisco, M., Ferguson, H. C., Koekemoer, A. M., et al. 2004, *ApJL*, 600, L93
- Gordon, K. D., Clayton, G. C., Misselt, K. A., Landolt, A. U., & Wolff, M. J. 2003, *ApJ*, 594, 279
- Greve, A. 2010, *A&A*, 518, A62
- Grogin, N. A., Kocevski, D. D., Faber, S. M., et al. 2011, *ApJS*, 197, 35
- Kennicutt, R. C., Jr., Calzetti, D., Walter, F., et al. 2007, *ApJ*, 671, 333
- Kessler, S., Leroy, A., Querejeta, M., et al. 1919, *ApJ*, 892, 23
- Koekemoer, A. M., Faber, S. M., Ferguson, H. C., et al. 2011, *ApJS*, 197, 36
- Kriek, M., & Conroy, C. 2013, *ApJL*, 775, L16
- Momcheva, I. G., Brammer, G. B., van Dokkum, P. G., et al. 2016, *ApJS*, 225, 27
- Narayanan, D., Conroy, C., Davé, R., Johnson, B. D., & Popping, G. 2018, *ApJ*, 869, 70
- Nelson, E. J., van Dokkum, P. G., Brammer, G., et al. 2012, *ApJL*, 747, L28
- Nelson, E. J., van Dokkum, P. G., Momcheva, I., et al. 2013, *ApJL*, 763, L16
- Osterbrock, D. E. (ed.) 1989, *Astrophysics of Gaseous Nebulae and Active Galactic Nuclei* (Sausalito, CA: Univ. Science Books)
- Papovich, C., Rudnick, G., Rigby, J. R., et al. 2009, *ApJ*, 704, 1506
- Pei, Y. C. 1992, *ApJ*, 395, 130
- Petersen, L., & Gammelgaard, P. 1997, *A&A*, 323, 697
- Puxley, P. J., & Brand, P. W. J. L. 1994, *MNRAS*, 266, 431
- Salim, S., & Narayanan, D. 2020, *ARA&A*, 58, 529
- Salmon, B., Papovich, C., Long, J., et al. 2016, *ApJ*, 827, 20
- Shipley, H. V., Papovich, C., Rieke, G. H., Brown, M. J. I., & Moustakas, J. 2016, *ApJ*, 818, 60
- Simons, R. C., Papovich, C., Momcheva, I., et al. 2021, *ApJ*, 923, 203
- Skelton, R. E., Whitaker, K. E., Momcheva, L. G., et al. 2014, *ApJS*, 214, 24
- van der Wel, A., et al. 2012, *ApJS*, 203, 24
- Walter, F., Weiss, A., Scoville, N., et al. 2002, *ApJL*, 580, L21
- Weiner, B. J., et al. 2007, *ApJL*, 660, L39
- Wirth, G. D., et al. 2004, *AJ*, 127, 3121